# 125Mbps Ultra-Wideband System Evaluation for Cortical Implant Devices

Yi Luo[1], Chris Winstead[1] and Patrick Chiang[2]

*Abstract*—**This paper evaluates the performance of a 125Mbps Impulse Ratio Ultra-Wideband (IR-UWB) system for cortical implant devices by using low-$Q$ inductive coil link operating in the near-field domain. We examine design tradeoffs between transmitted signal amplitude, reliability, noise and clock jitter. The IR-UWB system is modeled using measured parameters from a reported UWB transceiver implemented in 90nm-CMOS technology. Non-optimized inductive coupling coils with low-$Q$ value for near-field data transmission are modeled in order to build a full channel from the transmitter (Tx) to the receiver (Rx). On-off keying (OOK) modulation is used together with a low-complexity convolutional error correcting code. The simulation results show that even though the low-$Q$ coils decrease the amplitude of the received pulses, the UWB system can still achieve acceptable performance when error correction is used. These results predict that UWB is a good candidate for delivering high data rates in cortical implant devices.**

## I. INTRODUCTION

Cortical implant devices have been explored and researched by scientists and engineers since the late 1950s for envisioned possibility to rehabilitate a variety of neural injuries by means of microelectrodes implanted within the central nervous system [1]. One of the most attractive applications is visual prosthesis which is intended to restore functional vision in those suffering from partial or total blindness. The main challenges of such a system are the requirements of high data rate and low power consumption. A minimum data rate of 20Mb/s is recommended for restoring functional vision [2]. The implanted system should be operated with a power density no greater than $0.8mW/mm^2$ to avoid tissue damage through heating effects [3].

Most cortical implant devices receive data through a mutual inductance channel, in which a coil is implanted inside the body. The implanted coil is coupled to an external coil placed against the skin. By stimulating the external coil, signals are induced in the implanted coil, which allows deliver of data to the implanted device. To date, most of the implantable devices used narrow-band modulations such as ASK, FSK or PSK, which achieve data rates up to 2.5 Mb/s [2] [4]. More recently, a data rate of 10.2 Mb/s was demonstrated using Pulse Harmonic Modulation (PHM) [5], which is also a narrow-band technique that exploits self resonance of the coils used to create the inductive data channel.

[1]Y. Luo and C. Winstead are with the Department of Electrical and Computer Engineering, UMC 4120, Utah State University, Logan, UT 84322 `chris.winstead at usu.edu`

[2]P. Chiang is with the Department of Electrical and Computer Engineering, 4103 Kelley Engineering Center, Oregon State University, Corvallis, OR 97331-5501. `pchiang at eecs.oregonstate.edu`

The IR-UWB has been a promising candidate for cortical implant system because of its high data rates (usually several hundred Mbps), low complexity, and low power consumption. IR-UWB transmission has been proposed for transmitting data into cortical implants [6], and for backward telemetry from the implanted device [7]. To date there has not been a thorough investigation of IR-UWB for forward communication into cortical implant devices, since the UWB technique is proposed to be used in far-field domain, but the signal which is in 3.1–10.6 GHz band is highly absorbable *in vivo* in such domain and is hard to pass through human tissue conductor [8], [9]. In this paper, we evaluate the feasibility of IR-UWB communication in near-field domain based on the measured characteristics of a 3–5 GHz UWB transceiver. We show that this transceiver can be adapted for use in cortical implants.

In an IR-UWB system, the data is modulated as a train of sub-nanosecond pulses. Several researchers used the near-field inductive links to transmit narrow pulses in applications such as contact-less chip testing and body area networks [10]. To transmit wideband data, both the TX and RX coils require large self-resonance frequencies (SRF) to allow the high-frequency components of the narrow pulses pass through the inductive link. But it is quite challenging to implement such wideband coils since the parasitic capacitance around the coils is large due to the high conductivity of the body tissue [11]. One solution to this problem is lowering the coils' quality factor ($Q$) by adding series or parallel resistors. Some researchers have argued that low-$Q$ coils are unsuitable for implantable devices since the amplitude of the received signal will be reduced because of low $Q$ value, thus degrading the signal-to-noise ratio (SNR) at the receiver [5], [11]. But to the author's knowledge, it has not been explicitly reported the extent to which the low-$Q$ coils affect the system performance.

In this paper, we evaluate the performance of a 125Mbps IR-UWB system, in which the wideband data pulses are transmitted in near-field domain using low-$Q$ inductive coils. This IR-UWB system is modeled using measured parameters from a reported UWB transceiver implemented in 90nm-CMOS technology. The transfer functions between all the coils are analyzed to predict the signal attenuation and power interference. All possible dominant noise sources and clock jitters are considered. We show that the coil attenuation and clock jitter are effectively corrected by using a low-complexity error correcting code.

## II. SYSTEM ARCHITECTURE AND MODELING

The proposed UWB cortical implant system diagram is depicted in Fig. 1. The system consists of two mutual-inductor
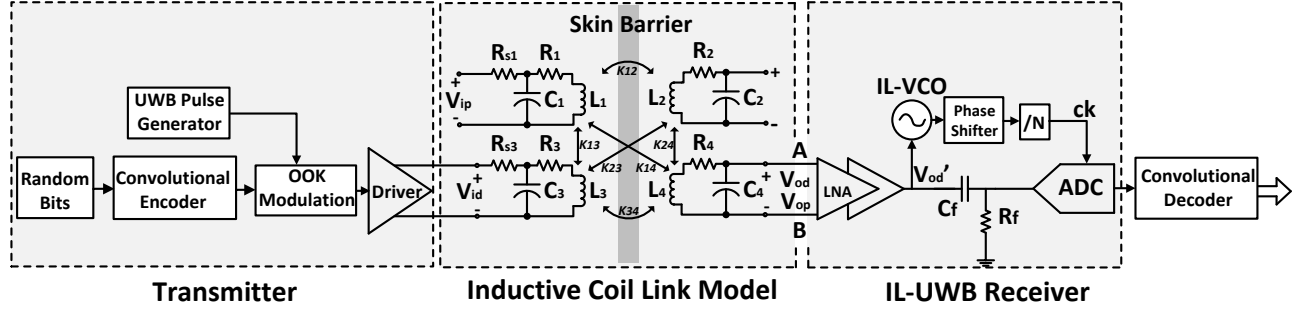
Fig. 1: Near-field data transmission system: Transmitter, Inductive Coil Link, and IL-UWB Receiver.

interfaces: one pair to deliver power into the implanted device ($L_1$:$L_2$), and a second pair to deliver data ($L_3$:$L_4$). These pairs of coils can be made approximately independent of each other, so that the data channel is isolated from the power channel. In practice, there is likely to be a small mutual inductance between all four coils, leading to potential interference. We therefore account for all mutual inductances in this analysis.

The transmitted data is encoded by a convolutional encoder with rate 1/2, i.e. the encoder adds one parity-check bit for each data bit. The encoded data sequence is modulated using On-Off Keying (OOK). The driver injects a train of OOK-modulated UWB pulses into the transmit coil ($L_3$). The transmitted pulse chain $V_{id}$ passes through the inductive coil link, stimulating an output signal $V_{od}$ on the terminals of $L_4$. A power interference contribution, $V_{op}$, also appears at $L_4$ and is superimposed on $V_{od}$. After being received by the UWB receiver, the data is processed by the convolutional decoder, and the original data bits are recovered.

### A. Transmitter Model

The transmitter consists of a convolutional encoder and a UWB pulse generator. For this work, we chose a low-complexity $R = 1/2$ convolutional encoder with generator polynomial $G(x) = \begin{bmatrix} 1+x^2 & 1+x+x^2 \end{bmatrix}$. After encoding, the data is modulated as an train of Gaussian-derivative pulses. We use the Scholtz's monocycle pulse in this evaluation [12] with a 1ns pulse width, as shown in Fig. 2(a) (the amplitude has been normalized to $1V$).

### B. Inductive Coil Link

The lumped model for the inductive coil link is also illustrated in Fig. 1. The coupling coefficients $k_{ij}$ between coils $L_i$ and $L_j$ are reported in Table I. The central frequency of the data coil is $f_d = 4$GHz (or close to it). The carrier frequency of the power coil $f_p$ is typically in the range of 1–10MHz [6]. In this work, we assume $f_p = 1$MHz.

*1) Coil Parameters:* We use two pairs of coils to transmit power and data separately, since if only one pair of coil is used for both power and data transmission at the same time, it requires extremely wide bandwidth in order to transmit the UWB signals and hence result in a much lower $Q$ value, leading to the severe reduction of power efficiency.

Several papers have described coil design procedures for cortical implants [7], [13]–[16]. In this work, we adopted dimensions parameters reported by Jow [14] for power coils, and designed the data coils exclusively for UWB transmission. The $L/R/C$ values of coils and coupling coefficients are shown in Table I. $R_4$ is designed to be a large value in order to decrease the quality factor $Q$. By using a low-$Q$ design, we obtain a flat frequency response which minimizes inter-symbol interference (ISI) in the transmitted pulses.

It should be noted that the data coils presented here are non-optimized, i.e. the undesired cross coupling coefficients($k_{13}$, $k_{14}$, $k_{23}$ and $k_{24}$) are not minimized, thus the power interference is not minimized.

TABLE I: $L/R/C$ values and coupling coefficients of the inductive link coils.

| Parameter | Coils in this work | | | |
|---|---|---|---|---|
| | $L_1$* | $L_2$* | $L_3^{\diamond}$ | $L_4^{\diamond}$ |
| $L_i(\mu H)$ | 25.71 | 29.51 | 0.16 | 0.13 |
| $C_i$ | $0.99nF$ | $0.86nF$ | $10.12fF$ | $12.25fF$ |
| $R_i(\Omega)$ | 6.94 | 10.62 | 1.83 | 2000 |

| $k_{12}$ | $k_{34}$ | $k_{14}$ | $k_{13}$ | $k_{23}$ | $k_{24}$ |
|---|---|---|---|---|---|
| 0.2322 | 0.0841 | 0.0056 | 0.0319 | 0.0061 | 0.0092 |

\* The dimensions are the same with the design in [14].
$\diamond$ Designed for UWB data transmission using the method of Jow and Ghovanloo [14].

*2) Transfer Function:* We denote the signal path from $L_i$ to $L_j$ as $P(ij)$. The data signal paths from $V_{id}$ to $V_{od}$ include path $P(34)$, $P(314)$ and $P(324)$, with corresponding transfer functions $H_{34}$, $H_{314}$, $H_{324}$, and impulse responses $h_{34}$, $h_{314}$, $h_{324}$, respectively. The power signal paths from $V_{ip}$ to $V_{op}$ include path $P(14)$, $P(134)$ and $P(124)$, with corresponding transfer functions $H_{14}$, $H_{134}$, $H_{124}$, and impulse responses $h_{14}$, $h_{134}$, $h_{124}$, respectively. Since $L_{1,3}$ are loosely coupled(small $k$) with $L_4$ and the current in tank $L_4C_4$ is very small, we can neglect the effect of $L_4C_4$ loading on the tank $L_1C_1$ and $L_3C_3$ to simplify the equations [11]. The transfer functions in the S-domain are deduced as follows:

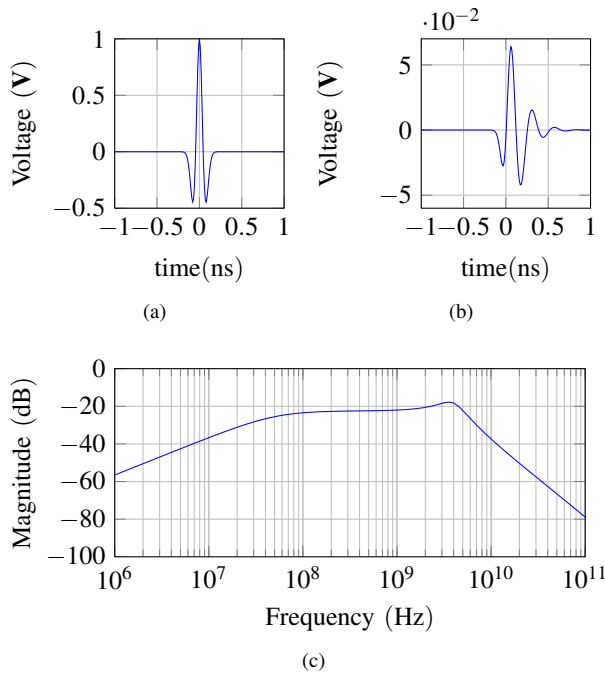$$H_{i4}(s) = \frac{M_{i4}s}{D_i(s) \cdot D_4(s)}, \quad i = 1,3 \tag{1}$$

Fig. 2: (a) A tansmitted pulse. (b) A received pulse by coil $L_4$. (c) Bode diagram of $H_{34}$.

$$H_{j24}(s) = \frac{-M_{j2}M_{24}C_2 s^3}{D_j(s) \cdot D_2(s) \cdot D_4(s)}, \quad j = 1, 3 \qquad (2)$$

$$H_{ij4}(s) = \frac{-M_{13}M_{j4}R_{sj}C_j s^3 + M_{13}M_{j4}s^2}{D_1(s) \cdot D_3(s) \cdot D_4(s)}$$
$$(i, j) = (1, 3) \, \text{or} \, (3, 1) \quad (3)$$

where

$$D_1(s) = R_{s1}L_1C_1 s^2 + (R_{s1}R_1C_1 + L_1)s + (R_1 + R_{s1})$$
$$D_2(s) = L_2C_2 s^2 + R_2C_2 s + 1$$
$$D_3(s) = R_{s3}L_3C_3 s^2 + (R_{s3}R_3C_3 + L_3)s + (R_3 + R_{s3})$$
$$D_4(s) = L_4C_4 s^2 + R_4C_4 s + 1$$

Fig. 2(b) shows one received pulse at the input of the low-noise amplifier (LNA) when the transmitted pulse is in Fig. 2(a). Fig. 2(c) shows the bode plot of data transfer function $H_{34}$.

### C. UWB Receiver

The extremely short pulses used for UWB modulation require very precise synchronization and fast switching times in both the Tx and Rx circuits. Hu *et al.* demonstrated a UWB architecture using pulse Injection-Locking (IL) to achieve phase synchronization [17]. This injection-locking UWB receiver (IL-UWB) eliminates the clock/data recovery (CDR) circuitry and multiplexer that are commonly used in UWB systems.

Furthermore, the ADC can run at the actual data rate so that the sampling requirements can be relaxed and the power consumption is significantly reduced. In Hu's demonstration, the receiver consumed 90pJ/bit at a data rate of 125MHz.

*1) Operation Principle:* As depicted in Fig. 1, after the inductive link transmission, the received data $V_{od}$ is passed through the IL-UWB system. It is first amplified by a two-stage LNA, then is directly injected into an injection-locked VCO (IL-VCO), which provides sample timing for a 2-bit flash ADC.

*2) Jitter and Noise:* The reported RMS sampling clock jitter measured in Hu's IL-UWB receiver is 8.0 picoseconds (ps) when the data rate is 125Mbps [17]. In our evaluation, jitter is modeled as a Gaussian-distributed random error in the received pulse sampling time. As shown in Sec. III, sampling jitter has the dominant influence in reducing the receivers' reliability. In addition to the jitter, a number of secondary noise contributions were included in our simulations. One main noise source is the LNA. The LNA's noise figure (NF, in dB) is a measure of degradation of SNR. The NF of the LNA is not mentioned in [17], but it is typically less than 5dB [18]–[20]. In our simulations, we consider the range of 4–6 dB to account for the impact of LNA noise on the reliability of the system. The thermal noise contributions are also modeled for all resistors and coils in the system.

### III. RESULTS

Simulations were performed using the model details described in Sec. II. In our simulations, the bit error rate (BER) was evaluated as the primary measure of system reliability performance. Fig. 3 shows the system performance when the LNA noise figure is 4dB, 5dB and 6dB. For each plot, the RMS sampling jitter is 8.0ps.
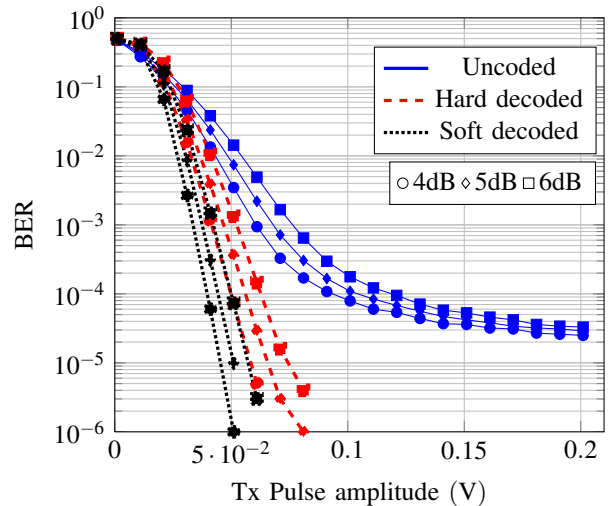


Fig. 3: System performance when LNA NF=4dB, 5dB, 6dB; jitter-RMS = 8.0ps.

Fig. 4 shows the system performance when the RMS of jitter is 7.0ps, 8.0ps and 9.0ps, while the LNA noise figure is

constant at 5dB.

The results shown in Figs. 3 and 4 indicate that the system cannot function reliably without the use of error correction. In particular, Fig. 4 demonstrates that sampling jitter plays the major limiting role in this system. Sampling jitter creates an *error floor* that limits the system's reliability, independent of pulse amplitude. By using the convolutional error correction code, the error floor is effectively eliminated.

In order to realize the proposed system, the remaining challenge is to demonstrate an implementation of the convolutional decoder that satisfies the power constraints of implanted devices. To meet this requirement, analog decoding circuits may potentially be used, which have been demonstrated with power as low as 40pJ/bit [21].
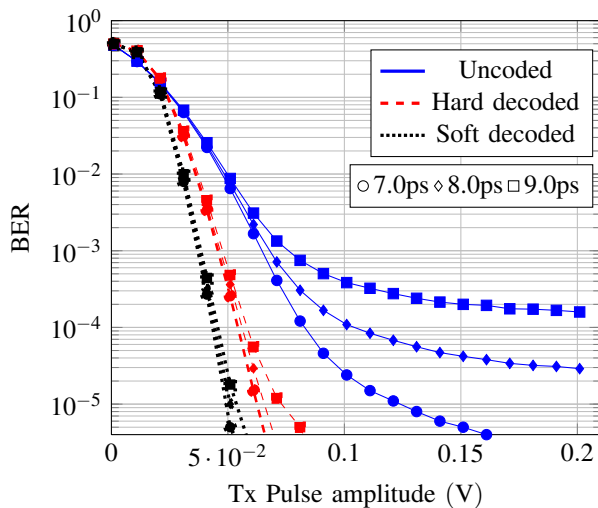


Fig. 4: System performance when jitter-RMS=7.0ps, 8.0ps, 9.0ps; LNA NF=5dB.

## IV. CONCLUSIONS

In this paper, we evaluated the performance of a 125Mbps IR-UWB system for cortical implant devices by using a low-$Q$ inductive coil link in the near-field domain. Large resistors are added to the data coils to lower the $Q$ value. Using measured parameters from a previously reported injection-locking UWB receiver, we performed simulations to evaluate the feasibility and reliability of a UWB cortical interface operating at 125Mbps. Dominant sources of noise, timing jitter and pulse filtering are included in the evaluation.

From the simulation results, we conclude that even though the low-$Q$ coils introduce significant attenuation of the received pulses, the system can still achieve acceptable performance if error correction is applied. The synchronization accuracy of IR-UWB system has the dominant impact on the receiver's BER, but this effect is removed by the error correcting operation. Based on this evaluation, we predict that the UWB technique is a promising candidate for delivering very high data rates to cortical implant devices.

## REFERENCES

[1] R. C. Gesteland, B. Howland, J. Y. Lettvin, and W. H. Pitts, "Comments on microelectrodes," *Proceedings of the IRE*, vol. 47, no. 11, pp. 1856–1862, 1959.

[2] C. T. Charles, "An implantable i-uwb transceiver architecture with power carrier synchronization," in *Proc. IEEE Int. Symp. Circuits and Systems ISCAS 2008*, 2008, pp. 1970–1973.

[3] S. G. D. C. Seese TM, Harasaki H, "Characterization of tissue morphology, angiogenesis, and temperature in the adaptive response of muscle tissue to chronic heating." *Lab Invest*, vol. 78(12), pp. 1553–1562., 1998 Dec.

[4] M. Ghovanloo and K. Najafi, "A wideband frequency-shift keying wireless link for inductively powered biomedical implants," *IEEE Transactions on Circuits and Systems—Part I: Regular Papers*, vol. 51, no. 12, pp. 2374–2383, 2004.

[5] F. Inanlou, M. Kiani, and M. Ghovanloo, "A 10.2 mbps pulse harmonic modulation based transceiver for implantable medical devices," *IEEE Journal of Solid-State Circuits*, vol. 46, no. 6, pp. 1296–1306, 2011.

[6] C. T. Charles, "Wireless data links for biomedical implants: Current research and future directions," in *Proc. IEEE Biomedical Circuits and Systems Conf. BIOCAS 2007*, 2007, pp. 13–16.

[7] U.-M. Jow and M. Ghovanloo, "Optimization of data coils in a multiband wireless link for neuroprosthetic implantable devices," *IEEE Transactions on Biomedical Circuits and Systems*, vol. 4, no. 5, pp. 301–310, 2010.

[8] Y. Chan, M. Q.-H. Meng, K.-L. Wu, and X. Wang, "Experimental study of radiation efficiency from an ingested source inside a human body model*," in *Proc. 27th Annual Int. Conf. of the Engineering in Medicine and Biology Society IEEE-EMBS 2005*, 2005, pp. 7754–7757.

[9] J. C. Lin, A. W. Guy, and C. C. Johnson, "Power deposition in a spherical model of man exposed to i-20-mhz electromagnetic fields," *IEEE Transactions on Microwave Theory and Techniques*, vol. 21, no. 12, pp. 791–797, 1973.

[10] Y. Wang, A. M. Niknejad, V. Gaudet, and K. Iniewski, "A cmos ir-uwb transceiver design for contact-less chip testing applications," *IEEE Transactions on Circuits and Systems—Part II: Express Briefs*, vol. 55, no. 4, pp. 334–338, 2008.

[11] F. Inanlou and M. Ghovanloo, "Wideband near-field data transmission using pulse harmonic modulation," *IEEE Transactions on Circuits and Systems—Part I: Regular Papers*, vol. 58, no. 1, pp. 186–195, 2011.

[12] X. Chen and S. Kiaei, "Monocycle shapes for ultra wideband system," in *Proc. IEEE Int. Symp. Circuits and Systems ISCAS 2002*, vol. 1, 2002.

[13] M. Ghovanloo and S. Atluri, "A wide-band power-efficient inductive wireless link for implantable microelectronic devices using multiple carriers," *IEEE Transactions on Circuits and Systems—Part I: Regular Papers*, vol. 54, no. 10, pp. 2211–2221, 2007.

[14] U.-M. Jow and M. Ghovanloo, "Design and optimization of printed spiral coils for efficient transcutaneous inductive power transmission," *IEEE Transactions on Biomedical Circuits and Systems*, vol. 1, no. 3, pp. 193–202, 2007.

[15] ——, "Optimization of a multiband wireless link for neuroprosthetic implantable devices," in *Proc. IEEE Biomedical Circuits and Systems Conf. BioCAS 2008*, 2008, pp. 97–100.

[16] G. Wang, P. Wang, Y. Tang, and W. Liu, "Analysis of dual band power and data telemetry for biomedical implants," *IEEE Transactions on Biomedical Circuits and Systems*, no. 99, 2011, early Access.

[17] C. Hu, R. Khanna, J. Nejedlo, K. Hu, H. Liu, and P. Y. Chiang, "A 90 nm-cmos, 500 mbps, 3–5 ghz fully-integrated ir-uwb transceiver with multipath equalization using pulse injection-locking for receiver phase synchronization," *IEEE Journal of Solid-State Circuits*, vol. 46, pp. 1076–1088, 2011.

[18] Y. Lu, K. S. Yeo, A. Cabuk, J. Ma, M. A. Do, and Z. Lu, "A novel cmos low-noise amplifier design for 3.1- to 10.6-ghz ultra-wide-band wireless receivers," *IEEE Transactions on Circuits and Systems—Part I: Regular Papers*, vol. 53, no. 8, pp. 1683–1692, 2006.

[19] G. Sapone and G. Palmisano, "A 3–10-ghz low-power cmos low-noise amplifier for ultra-wideband communication," *IEEE Transactions on Microwave Theory and Techniques*, vol. 59, pp. 678–686, 2011.

[20] R. Baker, *CMOS Circuits Design, Layout, and Simulation, 3rd Edition*. A John Wiley & Sons, Inc., 2010.

[21] C. Winstead, N. Nguyen, V. Gaudet, and C. Schlegel, "Low-voltage cmos circuits for analog iterative decoders," *Circuits and Systems I: Regular Papers, IEEE Transactions on*, vol. 53, no. 4, pp. 829 – 841, april 2006.